THE JOURNAL OF COMPARATIVE NEUROLOGY 416:356–367 (2000)

Cell Mosaic Patterns in the Native and Regenerated Inner Retina of Zebrafish: Implications for Retinal Assembly

DAVID A. CAMERON[1]* AND LAUREL H. CARNEY[2]
[1]Department of Physiology, Boston University School of Medicine, Boston, Massachusetts 02118
[2]Department of Biomedical Engineering, Boston University, Boston, Massachusetts 02215

ABSTRACT

In part because of its laminar organization and morphologically distinct cell populations, the vertebrate retina has often been used as a system for investigating the assembly of neural structures. The retinas of adult teleost fish, because they grow throughout life and can regenerate following an injury, provide an especially attractive model system for such investigations. In an effort to provide a quantitative foundation for testing hypotheses regarding the mechanisms of pattern formation during growth and regeneration of the vertebrate retina, nearest neighbor and auto-correlation analyses were used to examine the mosaic patterns of eight inner retinal cell groups in the native and regenerated retina of adult zebrafish. In both native and regenerated retina, the mosaic patterns of most inner retinal cells are non-random. However, regenerated mosaics tend toward significantly lower nearest neighbor distances, less orderly patterns, and more variable radial locations than their native retina counterparts. The individual cell groups in both native and regenerated inner retina are likely to be spatially distributed independently. The results support the hypotheses that, in the adult zebrafish: 1) distinct inner retinal cell groups of native retina are also present in regenerated retina; 2) the assembly of inner retinal cell mosaics is controlled by non-random spatial organizing mechanisms during development, growth, and regeneration; and 3) the spatial organization of cell mosaics is disrupted during regeneration. The results suggest that retinal regeneration may represent a spatially disrupted recapitulation of retinal developmental mechanisms. J. Comp. Neurol. 416:356-367, 2000.

Indexing terms: ***Danio rerio*; regeneration; pattern formation; amacrine cells; bipolar cells; retinal ganglion cells**

The retinas of adult teleost fish, unlike those of most adult vertebrates, can regenerate neurons following retinal injury (review: Raymond and Hitchcock, 1997). This regenerative phenomenon shares features with normal retinal development and growth, suggesting that the neuroregenerative process may represent a recapitulation of developmental mechanisms that is somehow triggered by retinal damage. For example, following a surgical extraction of a portion of the neural retina, the regenerative process invokes an anomalous expression of Pax6 (Hitchcock et al., 1996), a gene implicated in eye development throughout the animal kingdom (Graw, 1996). Additionally, in retina that is regenerated following a surgical extraction of extant retina, the laminar organization (Hitchcock et al., 1992), synaptic apparatus and connectivity (Hitchcock and Cirenza, 1994; Cameron and Easter, 1995), dendritic attributes (Hitchcock, 1997; Cameron et al., 1999), and visual pigments (Cameron et al., 1997) are all similar to that of native retina.

In contrast, additional evidence suggests that the mechanisms that underlie retinal development and regeneration might, in some aspects, be significantly different. Unlike the circumferential germinal zone, from whence neurons are produced and added to the teleost retina throughout life, the regenerative blastema that forms after surgical extraction of retina is not stimulated to proliferate by insulin-like growth factors (Boucher and Hitchcock, 1998). Additionally, following retinal destruction by the cytotoxic

Grant sponsor: NIH; Grant number: EY11160.

*Correspondence to: David A. Cameron, Department of Physiology, Boston University School of Medicine, 80 East Concord Street, Boston, MA 02118. E-mail: dcameron@bu.edu

Received 10 June 1999; Revised 17 August 1999; Accepted 4 October 1999

agent ouabain, regenerated cells in central retina are thought to be produced by a surviving population of germinal cells that reside within the neural retina, called rod precursor cells, which normally only produce rod photoreceptors (Raymond et al., 1988).

In an effort to improve our understanding of cellular pattern formation during retinal growth and regeneration, and of the potential similarities and differences between these two neurogenerative processes, a quantitative analysis of retinal cell mosaic patterns in the adult zebrafish was performed. The two-dimensional mosaics of identified cell groups across the retinal sheet, including bipolar, amacrine, and retinal ganglion cells, were evaluated using nearest neighbor analysis and the density recovery profile method of Rodieck (1991). The location of cells within the radial depth of the native and regenerated retina was also examined qualitatively.

The results indicate that many inner retinal cell groups in both native and regenerated retina are organized into two-dimensional mosaics that are non-random. Compared to their native retina counterparts, however, the cellular mosaics of regenerated retina tend to have higher density and to be less regularly organized, with some cells being located at anomalous locations in the radial dimension, and sometimes being closely juxtaposed with another cell of the same group. In both native and regenerated retina the mosaics of unlike-neurons are largely independent of one another, suggesting that interactions between unlike inner retinal neurons may not contribute significantly toward the formation of their respective mosaic patterns. Based on these results, we argue that the assembly of cell mosaics in the inner retina is directed by non-random, spatial organizing mechanisms during retinal development, growth, and regeneration, and that these mechanisms are disrupted during retinal regeneration.

MATERIALS AND METHODS

Use of experimental animals conformed to the guidelines required by the Institutional Animal Care and Use Committee (IACUC) of Boston University School of Medicine. Adult zebrafish (*Danio rerio*) were purchased from local retail suppliers, and were communally housed in 5 gallon fish tanks. The fish used in this study had weights and standard lengths of 0.45 ± 0.17 g and 3.1 ± 0.4 cm, respectively (mean ± SD, $n = 21$). In an effort to control for cell mosaic attributes that might be dependent upon fish size or retinal hemifield, only similarly-size animals were used, and only cell mosaics derived from dorsal retina were analyzed, approximately half-way between the retinal margin and the optic nerve head.

Some fish ($n = 15$) were anesthetized (30–60 second immersion in 0.2% tricaine methanesulfonate; Sigma Chemical Co., St. Louis, MO), and a patch of approximately 0.25–0.5 mm^2 of dorsal retinal was removed surgically from the left or right eye, as described previously (Hitchcock et al., 1992; Cameron and Easter, 1995). Surgically treated fish were revived and returned to their home tanks, and the regenerated patches of dorsal retina were analyzed 75–228 days later.

Selective cell labeling

For analysis of cell mosaics in retinal whole mounts, light adapted animals were heavily anesthetized (3–5 minute immersion in 0.2% tricaine methanesulfonate), killed (aorta puncture), and eye cups isolated as described previously (Cameron and Easter, 1993). The eye cups were then placed in a fixative solution (0.25% picric acid/4% paraformaldehyde/0.1M PO_4, pH = 7.0) for 1 hour at room temperature, then overnight at 4°C. Whole mounts of the eye cups were then made, washed in phosphate buffered saline (PBS)/0.3% Triton-X (pH = 7.4), exposed to 10% normal goat serum (Sigma Chemical Co., St. Louis, MO)/PBS for 1 hour at room temperature, and then exposed to 1% primary antibody in PBS/10% normal goat serum/0.3% Triton-X/0.1% BSA on a shaker table at room temperature for 24 hours. For some experiments, retinas were simultaneously screened with two different primary antibodies; in these studies, only primary antibodies raised in different animals were utilized. The following antibodies were used in this study: mouse anti-tyrosine hydroxylase, rabbit anti-protein kinase C, and rat anti-serotonin (Chemicon, Temecula, CA); rabbit anti-serotonin, rabbit anti-somatostatin, rabbit anti-substance P, and rabbit anti-neuropeptide Y (DiaSorin, Stillwater, MN); rabbit anti-gamma aminobutyric acid (Sigma Chemical Co.). Following primary antibody exposure, the tissue was washed repeatedly in PBS and exposed to a 0.5–1.0% solution of Cy3- or Cy2-conjugated (Jackson ImmunoResearch, West Grove, PA), or TRITC- or FITC-conjugated (Sigma) secondary antibody in PBS against the primary antibody's source animal, for 24 hours at room temperature. The reacted tissue was then washed repeatedly with PBS, mounted on a glass slide (pigmented epithelium side down) with 50% glycerol/PO_4 buffer and a cover slip, and visualized with standard epifluorescence microscopy (Axioskop, Zeiss). In an effort to selectively label retinal ganglion cell somata in other retinas, optic nerves were completely transected close to the eye in anesthetized fish, and a pellet of tissue paper soaked in 15% propidium iodide/2% DMSO/dH_2O was placed in the eye socket. Animals were revived, and 30–60 minutes later the eyes were exposed to fixative (as above), and immediately prepared for epifluorescence microscopy. Because it intercalates with DNA, propidium iodide tends to collect within the nuclei of labeled cells, allowing their visualization with epifluorescence microscopy. All mounted retinas were stored at −20°C.

Photographs of labeled whole mounts were taken with a 35 mm camera system, and cell mosaics of labeled cells in dorsal retina were manually recorded using camera lucida. Estimates of cellular density were derived from circular areas superimposed upon each camera lucida rendering. The camera lucida renderings were digitized with a photoscanner (Scanjet 4C, Hewlett Packard), from which the location of each labeled cell was assigned a unique position in two-dimensional space (units in μm). For a given retinal field, the two-dimensional coordinate list of labeled cells was quantitatively analyzed (see below). Some retinas were also processed for cryosectioning, as described previously (Cameron and Easter, 1995). In these studies, sections were cut through the radial plane of the retina at approximately 30 μm thickness using a microtome cryostat (Model CTD, International Equipment Corp., Needham Heights, MA), mounted upon SuperFrost Plus glass slides (Bellco, Vineland, NJ), and stored at −20°C. Fluorescence immunochemistry of cryosections was similar to that described above, except that the antibody exposure times were performed in humidified chambers for 2 hours at room temperature. Because not all cells that share a common label are necessarily restricted to cells of the same

"type" (i.e., cells that are structurally and functionally identical), we refer to labeled cells that share a common marker as a "group" (see Rodieck, 1998). Additionally, the term "mosaic" is operationally defined in this report as referring to cells of a common group, rather than to cells of a common "type."

Nearest neighbor analysis

Nearest neighbor analysis is a technique used to characterize the pattern of objects in two or more dimensions, based upon each object's distance to its nearest neighboring object (Clark and Evans, 1954; Cook, 1996). Briefly, for each object in a sample, the direct distance to its nearest neighboring object in the same sample is recorded, independent of direction. The form of the nearest neighbor distance (NND) distribution was evaluated for randomness in the following ways. First, the ability of a Gaussian (normal) distribution to represent the NND distributions was evaluated with a χ^2 statistic. Second, the ratio of the mean to the standard deviation of these distributions was evaluated for significant difference from a theoretical random distribution using the "conformity ratio" method described by Cook (1996). Third, model NND distributions predicted for a uniformly distributed random distribution of two-dimensional points were determined for each cell group in two ways: application of the Rayleigh function described by Wässle and Riemann (1978), and a computer generated, two-dimensional uniform distribution of cells. In a uniform distribution the cells are randomly positioned, and all locations in the two-dimensional space are equally probable. The Rayleigh function, truncated at the smallest possible nearest neighbor distance (soma diameter) and then scaled to represent a probability distribution, was used to illustrate potential differences between the data and a theoretical, uniformly distributed, random distribution. The computer-generated, uniformly distributed random distributions were themselves evaluated for randomness using the conformity ratio analysis. The NND distributions for a given cell group in native and regenerated retina were statistically compared using an independent t-test.

Density recovery profile (DRP)

The Density Recovery Profile (DRP) method, developed by Rodieck (1991), provides a quantitative representation of mosaic pattern, with an emphasis upon the detection of anti-clustering. Briefly, in the DRP analysis, the distance and direction to each and every other object in the sample is measured for a given object in the mosaic. Many (but not all; see below) such objects in the sample are similarly analyzed, and the resultant two-dimensional mosaics are superimposed (i.e., each object becomes the central reference of its own derived mosaic, and all derived mosaics are directly superimposed). The density of objects in the resulting pattern, as a function of the annular distance from the central reference object, is then determined. In this way, the density of objects within the sample is "recovered" at relatively large distances from the reference object, and an object-free zone surrounding the central reference object in the sample can be inferred. Termed the "effective radius," this object-free zone corresponds to the cell-free distance for an equivalent step function of the neighbor distance function that has the equivalent "recovered" cellular density. In an effort to avoid edge effects in the DRP analysis, each examined mosaic was parceled into nine equal-area sectors, analogous to a tic-tac-toe diagram, and only those cells within the central sector were analyzed (see Rodieck, 1991). This procedure eliminated some cell groups from the DRP analysis, as there could be few, if any, cells located within the central sector for cell groups with intrinsically low spatial density. The DRP analysis used in this study was applied using a custom MatLab (Natick, MA) algorithm.

RESULTS

Identification of labeled cells

Previous studies of teleost retina have suggested that the antibodies utilized in this report would label distinct groups of retinal cells (review: Dowling, 1987). To confirm this assumption, Figures 1 and 2a show, in radial cryosections through native retina, cells that were labeled by each of the antibodies used in this study; a radial cryosection of propidium iodide-labeled cells is shown in Figure 3a. The stereotypical, coplanar location of labeled somata, the differential estimates of cellular densities (Table 1), and the differential patterns of labeled dendritic processes support the notion that each antibody selectively labeled a distinct group of retinal cell. These results also support the following assignments of labeled cell identity, as reported in earlier investigations of teleost retinas: anti-protein kinase C (PKC), ON-type bipolar cells (Fig. 1a; Suzuki and Kaneko, 1990); anti-GABA (Fig. 1b), anti-somatostatin (Fig. 1d), anti-substance P (Fig. 1e), anti-neuropeptide Y (Fig. 1f), and anti-serotonin (Fig. 2a), amacrine cells (Marshak et al., 1984; Yazulla et al., 1985; Yazulla, 1986; Ehinger and Dowling, 1987; Dowling, 1987); anti-tyrosine hydroxylase, interplexiform cells (Fig. 1c; Yazulla and Zucker, 1988); and retrograde application of propidium iodide, retinal ganglion cells (RGCs, Fig. 3a). Cells that were immunopositive for tyrosine hydroxylase (see Figs. 1c, 8d), somatostatin (Fig. 1d) and neuropeptide Y (Fig. 1f) were characterized by widespread, complex patterns of labeled dendritic processes. The qualitative, two-dimensional pattern of RGCs, in which groups of axons and somata are organized as oriented bundles across the retinal sheet, was similar to that described by Kock and Reuter (1978) for the crucian carp retina (arrowheads, Fig. 3b). The propidium iodide label was somewhat less selective in radial cryosections than in retinal whole mounts (cf. Fig. 3a,b), perhaps due to leaching of the propidium iodide during the cryosection processing.

Fig. 1. Immunopositive cells in native zebrafish retina. Each panel presents labeled cells visualized with epifluorescence microscopy in radial sections (top) and in whole mounts (bottom). INL, inner nuclear layer; IPL, inner plexiform layer. **a:** Anti-protein kinase C, with the immunopositive peri-somata region (arrowhead) and synaptic apparatus region (arrow) indicated. The whole mount view is at the level of the synaptic apparatus; fluorescent blood vessels are visible as the out-of-focus branching patterns. **b:** Anti-GABA. Note the strong immunoreactivity throughout the inner plexiform layer. **c:** Anti-tyrosine hydroxylase. In the radial section, note the immunopositive processes within the IPL and in the outer retina (asterisk); epi-somatic processes are also visible in the whole mount view. **d:** Anti-somatostatin. A complex array of immunopositive processes is visible throughout the whole mount view. **e:** Anti-substance P. The relatively faint immunoreactivity of somata (arrow) was typical for this particular antibody. **f:** Anti-neuropeptide Y. Like the anti-somatostatin cells, complex arrays of immunopositive processes within the IPL are visible.

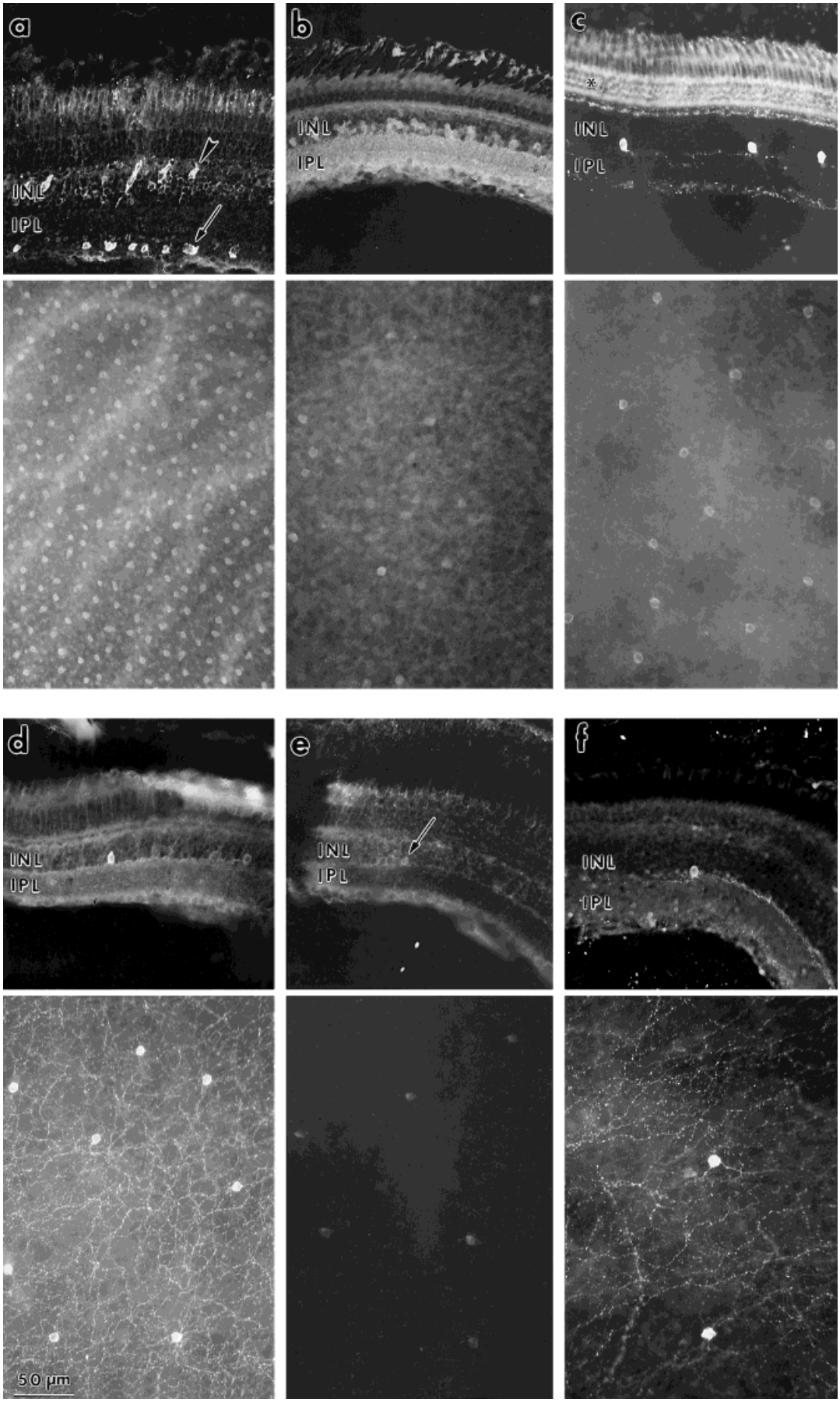

Figure 1

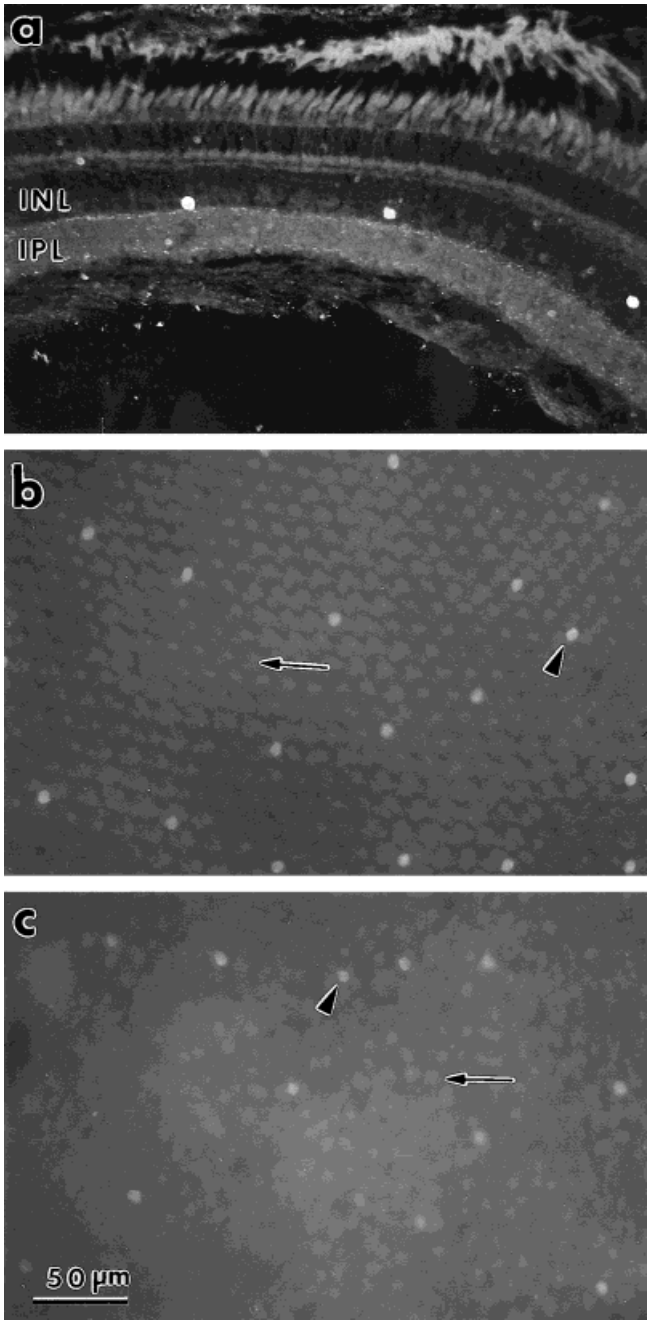

Fig. 2. Cells immunopositive for serotonin in the native and regenerated zebrafish retina. **a:** Anti-serotonin cells in a radial section of native retina. Note the immunopositive processes at both radial edges of the IPL. **b:** Double exposure view of a native retina whole mount screened with the anti-serotonin antibody. The anti-serotonin cells (arrowhead) are superimposed with an epifluorescence view of the underlying cones (arrow). Note the regular, orderly pattern of cone photoreceptors. Cone mosaics in teleost retinas can typically be directly visualized in retinal whole mounts with epifluorescence microscopy (Cameron and Easter, 1993). **c:** Double exposure view of anti-serotonin cells (arrowhead) and underlying cones (arrow) within regenerated retina. Note the disorderly cone mosaic compared to that observed in native retina (b).

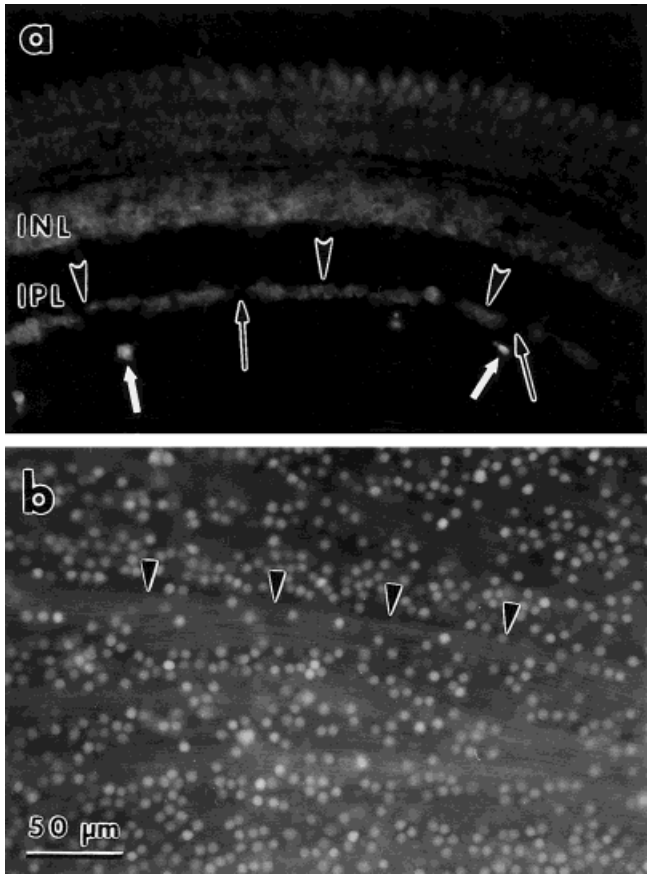

Fig. 3. Epifluorescence views of cells in the native zebrafish retina labeled via application of propidium iodide to the transected optic nerve. **a:** Propidium iodide-positive cells in a radial cryosection, at the level of retinal ganglion cell somata (arrowheads). Note that label is present within blood vessels (white arrows). Somata-free regions within the RGC layer are indicated (thin arrows). **b:** Propidium iodide-positive somata near the surface of a retinal whole mount. The optic nerve head is to the right, out of this field of view. Note the faintly labeled axons (arrowheads) that tend to be organized as oriented bundles between the propidium iodide-positive somata (the latter assumed to be RGCs). These regions were interpreted as corresponding to relatively somata-free regions, such as that indicated by the thin arrows in a.

These results suggest that each antibody and retrograde marker preferentially labels a unique set of neurons in the adult zebrafish retina. However, to avoid potential errors in cellular classification (e.g., due to the binding of a given antibody to multiple antigens), in this report each labeled cell group is typically referred to by the indicator antibody/marker.

Mosaic patterns in native retina

Representative cellular mosaic patterns for dorsal adult zebrafish retina are shown in the lower halves of each panel in Figure 1 (the data for serotonin-positive and propidium iodide-positive cells are shown on Figs. 2b and 3b, respectively). The cells of a given group were all largely coplanar, and the two-dimensional mosaics ranged from relatively high density (e.g., anti-PKC, Fig. 1a) to relatively low density (e.g., anti-neuropeptide Y, Fig. 1f). Estimates of planimetric density for each cell group are given in Table 1. For the anti-GABA-positive cells, which were not coplanar (Fig. 1b), care was taken to include for analysis only those cells located at the inner nuclear/inner plexiform layer boundary.

TABLE 1. Nearest Neighbor and DRP Parameters for Cells in the Native and Regenerated Inner Retina of Zebrafish[1]

Cell group	NND, μm mean ± SD (*n*)	Conformity ratio, data (mean/SD)	Conformity ratio, ran. (mean/SD)	Density, mm^{-2}	Effective radius, μm
PKC, nat	19.7 ± 3.6 (580)	5.47	1.82[2]	1,600 ± 100	15.4
PKC, reg	14.8 ± 4.2 (490)	3.52	1.86[2]	1,800 ± 525	9.7
GABA, nat[4]	36.1 ± 16.3 (320)	2.21	1.44[2]	225 ± 10	27.7
GABA, reg[4]	15.5 ± 4.6 (257)	3.37	1.90[2]	1,210 ± 650	8.9
5-HT, nat	50.2 ± 15.4 (453)	3.26	1.97[2]	177 ± 63	30.8
5-HT, reg	46.7 ± 16.8 (157)	2.78	1.66[2]	296 ± 119	51.2
TH, nat	78.1 ± 19.7 (302)	3.96	2.07[2]	89 ± 17	66.0
TH, reg	52.9 ± 22.9 (259)	2.31	1.69[2]	157 ± 49	41.1
som, nat	102.1 ± 29.8 (89)	3.43	1.89[2]	55 ± 14	n/a[3]
som, reg	60.4 ± 25 (214)	2.42	1.49[2]	149 ± 64	n/a[3]
sub P, nat	91.1 ± 33.9 (71)	2.69	1.66[2]	80 ± 33	n/a[3]
sub P, reg	36.7 ± 17.2 (28)	2.13[2]	1.89[2]	262 ± 46	n/a[3]
npY, nat	133.0 ± 65.3 (43)	2.04[2]	1.80[2]	19 ± 5	n/a[3]
npY, reg	122.3 ± 59.5 (14)	2.06[2]	1.45[2]	30 ± 3	n/a[3]
RGC, nat	8.2 ± 1.6 (356)	5.13	1.90[2]	7,800 ± 380	5.9
RGC, reg	7.4 ± 1.9 (825)	3.89	1.92[2]	10,250 ± 2,500	5.0

[1]Immunopositive cell group abbreviations as follows: PKC, protein kinase C; 5-HT, serotonin; TH, tyrosine hydroxylase; som, somatostatin; sub P, substance P; npY, neuropeptide Y. RGC indicates cells that were propidium iodide-positive; nat, native retina; reg, regenerated retina. Conformity ratios are given for the data and for a corresponding, randomly generated mosaic (ran) at equal density.
[2]Random pattern, based upon Figure 2 of Cook (1996).
[3]n/a, Data not available.
[4]Care was taken to restrict analysis to those anti-GABA-positive cells at the boundary between the inner nuclear and inner plexiform layers (see Results).

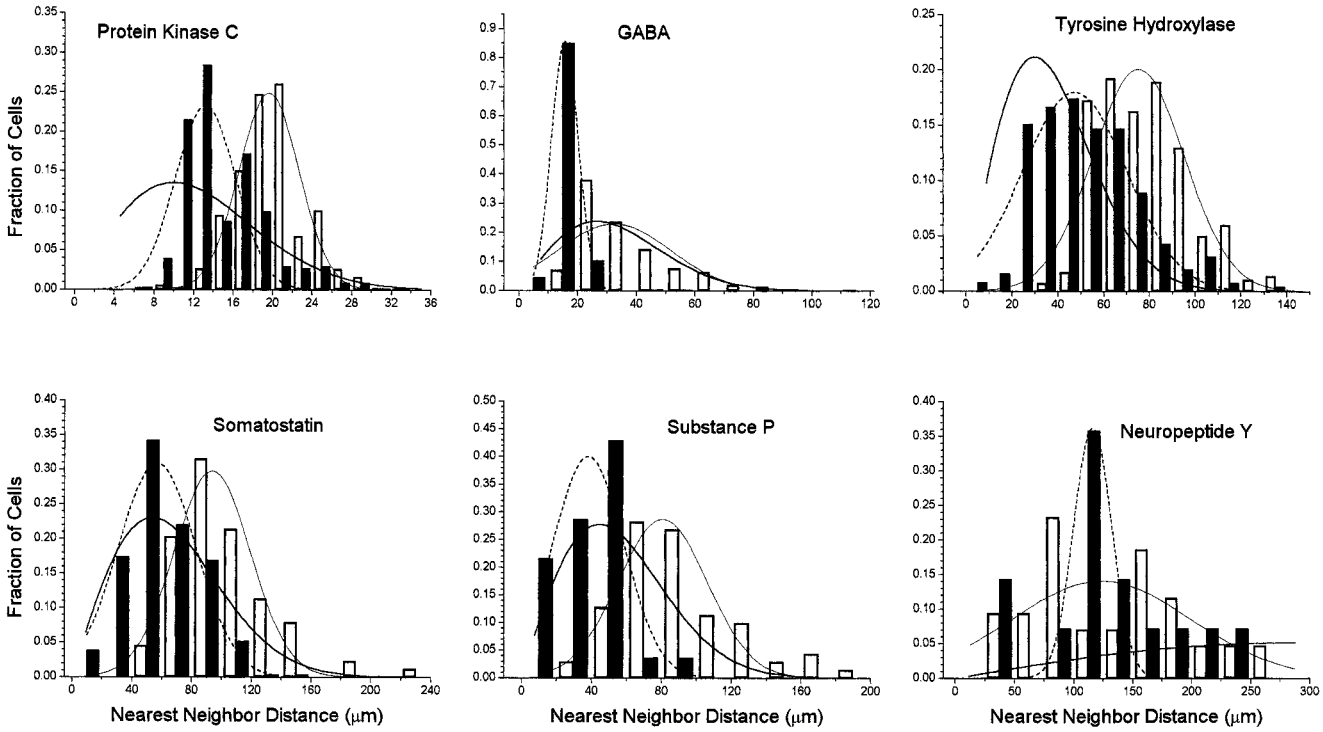

Fig. 4. Nearest neighbor distance (NND) distributions of inner retinal cells in native and regenerated zebrafish retina. The antibody marker is indicated for each panel. Open bars, native retina; filled bars, regenerated retina. Each NND distribution was fit with a Gaussian function, indicated by the thin solid and dashed lines (native and regenerated retina, respectively). The expected Rayleigh distribution derived for each native retina NND distribution is indicated by the thick solid line (Eq. 2 of Wässle and Riemann, 1978), truncated at the minimum possible NND, which was defined as the estimated soma diameter for that particular cell group (Figs. 1– 3).

The NND distributions for each labeled, native cell group in Figure 1 are plotted as the open bars in Figure 4, with a Gaussian function fit to the data (thin solid lines, Fig. 4). The NND distributions for serotonin-positive and propidium iodide-positive cells are shown on Figure 5. Because the Gaussian functions provided good estimates of most NND distributions (thin solid lines, Figs. 4 and 5), the hypothesis that the NND values were distributed normally could not be ruled out ($P > 0.05$, χ^2 test). In contrast, the expected NND distribution for a uniformly distributed random mosaic of cells, based upon the Rayleigh function described by Wässle and Riemann (1978; thick solid line in each panel of Fig. 4, truncated for each cell group's average soma diameter and scaled to represent a probability distribution) was typically a poor estimate of the NND distributions.

The mean ± SD values for each cell group's NND distribution are given in Table 1, and by the open bars on Figure 6a. Conformity ratio analysis (which utilizes the ratio of the mean and the standard deviation of the NND distribution; Cook, 1996) indicated that all the cell mosaics from native retina, with the exception of anti-neuropeptide

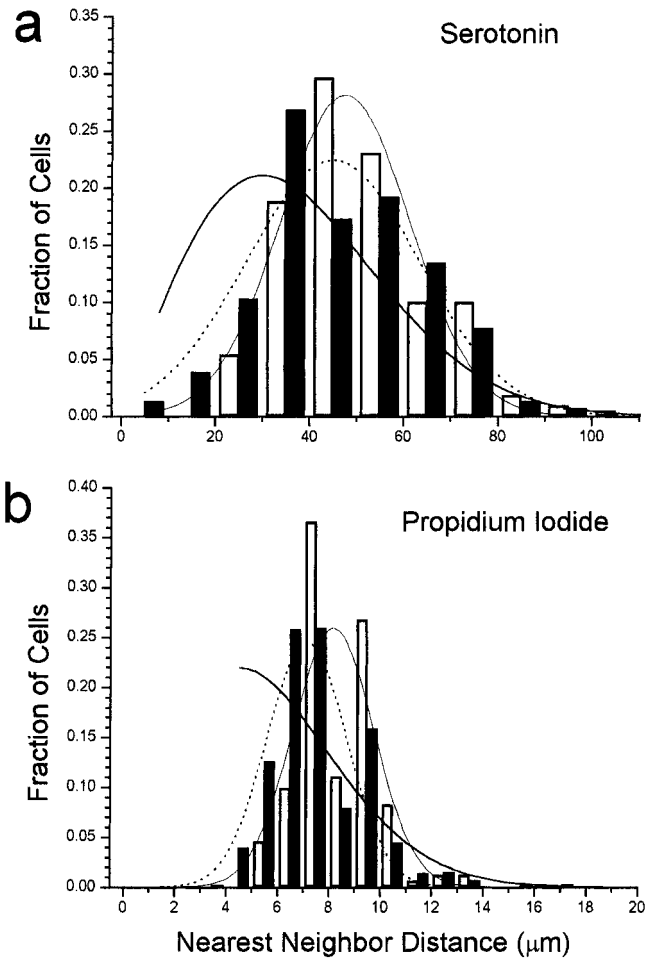

Fig. 5. **a,b:** NND distributions for anti-serotonin- and propidium iodide-positive cells in native and regenerated zebrafish retina. Symbols and lines are as in Figure 4.

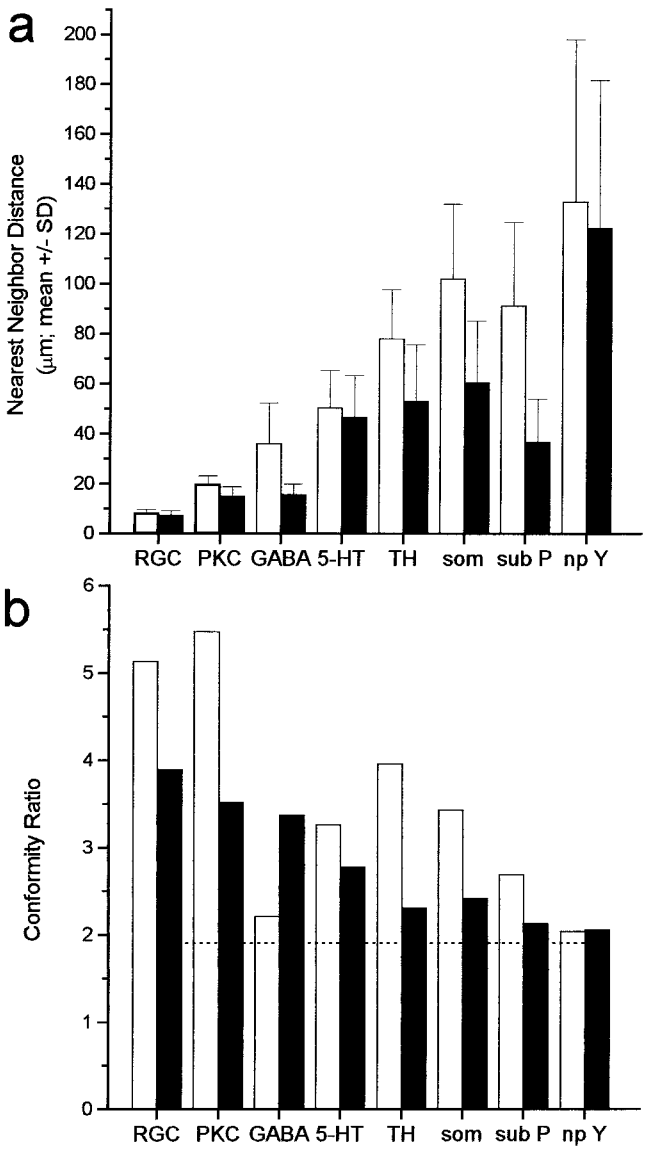

Fig. 6. Nearest neighbor distances and conformity ratios for inner retinal cells in native (open bars) and regenerated (filled bars) zebrafish retina. **a:** Mean ± SD values for the NND distributions illustrated in Figures 4 and 5. Except for the neuropeptide Y-positive cells, all native and regenerated NNDs for a given cell group were significantly different ($P < 0.05$, independent t-test; Table 1). **b:** Conformity ratios for each labeled cell group, defined as the mean/SD ratio of the NND distribution. Based upon the analysis of Cook (1996), the NND distribution for each cell group (except as noted in Table 1) is significantly different from that expected for a random distribution of cells. Dotted line, theoretical mean conformity ratio for a random group (Cook, 1996).

Y-positive cells, were significantly different from uniformly distributed random distributions ($P < 0.05$; open bars, Fig. 6b). The sparse density of neuropeptide Y-positive cells across the retina may have hindered mosaic pattern analysis using this technique. Computer-generated, uniformly distributed random distributions, matched to the intrinsic density of the corresponding cell group, always had conformity ratio values that were less than the data values, and were always similar to the value for theoretical random distributions (Table 1; Cook, 1996). Together, these results support the hypothesis that, in native zebrafish retina, the two-dimensional mosaic patterns of many inner retinal cells are not uniformly distributed (i.e., random).

The DRP analysis could only be applied to propidium iodide-, PKC-, GABA-, serotonin-, and tyrosine hydroxylase-positive cells; the relatively low density of the other cell groups precluded DRP analysis (see Materials and Methods). For those mosaics amenable to the DRP analysis, with the exception of propidium iodide-positive cells, the results indicated that each mosaic pattern was characterized by anti-clustering. This anti-clustering phenomenon was inferred by the calculated "effective radius" (dashed vertical lines, Fig. 7; Table 1), a circular region of two-dimensional space immediate to each somata, with a radius about 3–9 times larger than the soma diameter (dot-dashed vertical lines, Fig. 7; cf. Figs. 1 and 2), within which no like-cell soma was likely to be located. The effective radius for propidium iodide-positive cells was only slightly larger than the estimated soma (i.e., nuclear) diameter of these cells, consistent with the spoke-like clustering of these cells across the retinal sheet, as evident in Figure 3b. The results from the DRP analysis are thus

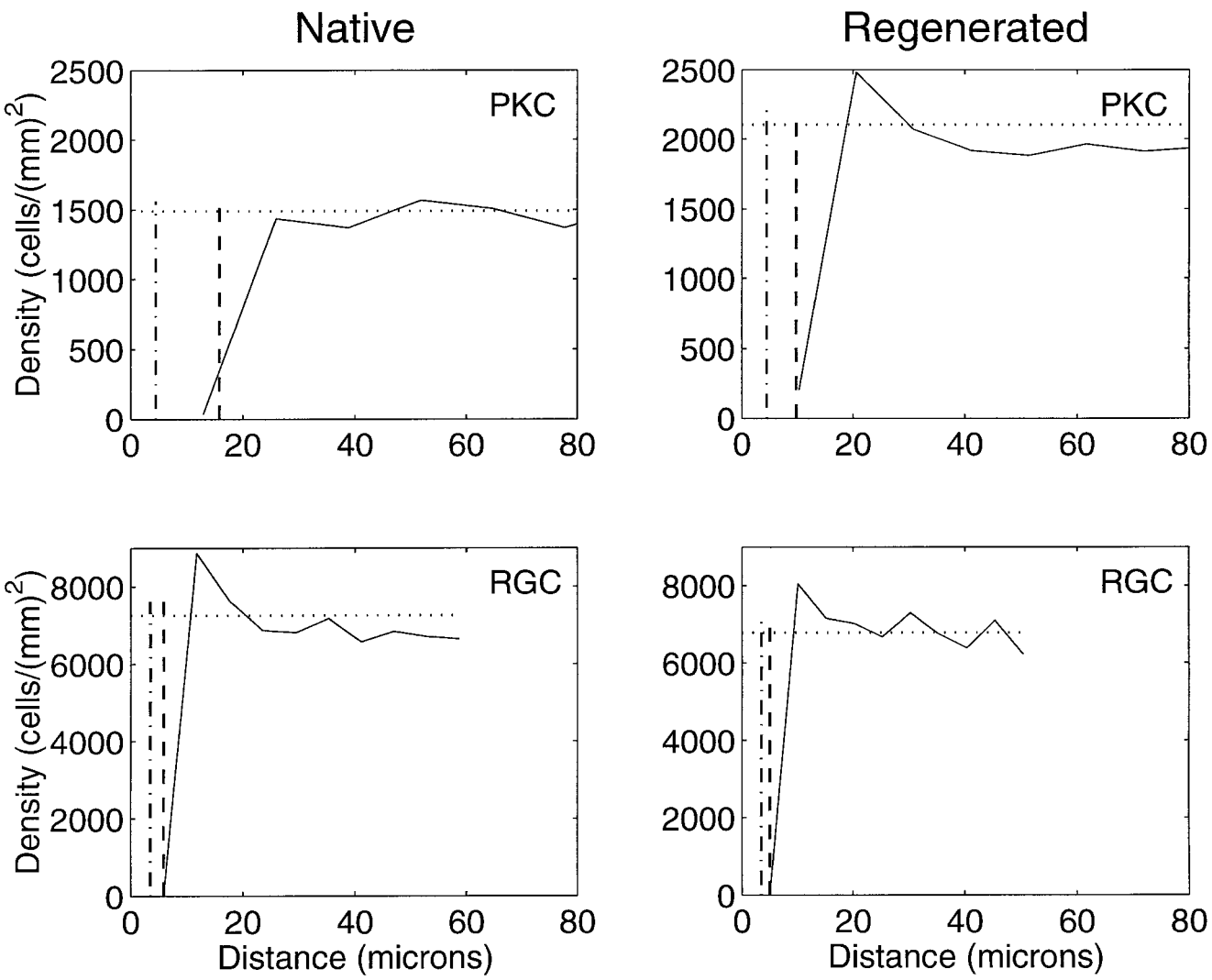

Fig. 7. Density recovery profile (DRP) analysis of inner retinal cell mosaics in native and regenerated zebrafish retina. The graphical format is based upon that of Rodieck (1991). DRPs are shown for anti-PKC-positive and propidium iodide-positive cells (PKC and RGC, respectively) in native and regenerated retina. In each plot the "recovered" cellular density is plotted as the horizontal dotted line; the vertical dashed line indicates the calculated "effective radius" value for that particular cell group; the left-most vertical line (alternating dash-dot) represents the cell group's somatic diameter (nuclear diameter in the case of RGCs). The solid line represents the calculated cell density as a function of distance from the center reference cell (see Materials and Methods).

consistent with the NND analyses in suggesting that the two-dimensional mosaic patterns of inner retinal cells in native zebrafish retina are non-random. The DRP results additionally suggest that the assembly of most inner retinal cell mosaics might involve the operation of some factor(s) that lessen the probability of proximal like-cells.

NND analysis was used to determine if the cell mosaics of distinct cell groups were independent of one another. For this analysis retinas that were screened with two different primary antibodies were examined. Within a given field of view, NND measurements were made for each labeled cell of group "A" to a labeled cell of group "B," and vice versa. The NND mean ± SD and conformity ratios for three cell pairs that were successfully labeled in both native and regenerated retinas are indicated in Table 2; the NND distributions between anti-somatostatin- and anti-tyrosine hydroxylase-positive cells are shown in Figure 8a. In each case, the conformity ratio for unlike-cells

TABLE 2. NND Analysis of Unlike Cell Groups in the Native and Regenerated Inner Retina of Zebrafish[1]

Cell group pair		NND (μm) mean ± SD (*n*)	Conformity ratio
TH → 5HT	nat:	51.1 ± 36.8 (173)	1.39[2]
	reg:	38.6 ± 28.8 (63)	1.34[2]
5HT → TH	nat:	50.3 ± 22.5 (275)	2.24[3]
	reg:	43.6 ± 27.3 (81)	1.60[2]
TH → som	nat:	88.6 ± 48.4 (67)	1.83[2]
	reg:	95.7 ± 55.7 (72)	1.72[2]
som → TH	nat:	47.6 ± 20.7 (25)	2.30[2]
	reg:	41.7 ± 24.1 (20)	1.73[2]
PKC → TH	nat:	31.2 ± 12.4 (67)	2.52[4]
	reg:	43.1 ± 19.4 (139)	2.22[5]

[1]NND distribution mean ± SD and conformity ratios as in Table 1. Symbols appended to the conformity ratio values indicate the following criterion levels for non-randomness, from Figure 2 of Cook (1996): [2], random; [3], non-random at $P < 0.001$; [4], non-random at $P < 0.01$; [5], non-random at $P < 0.05$.

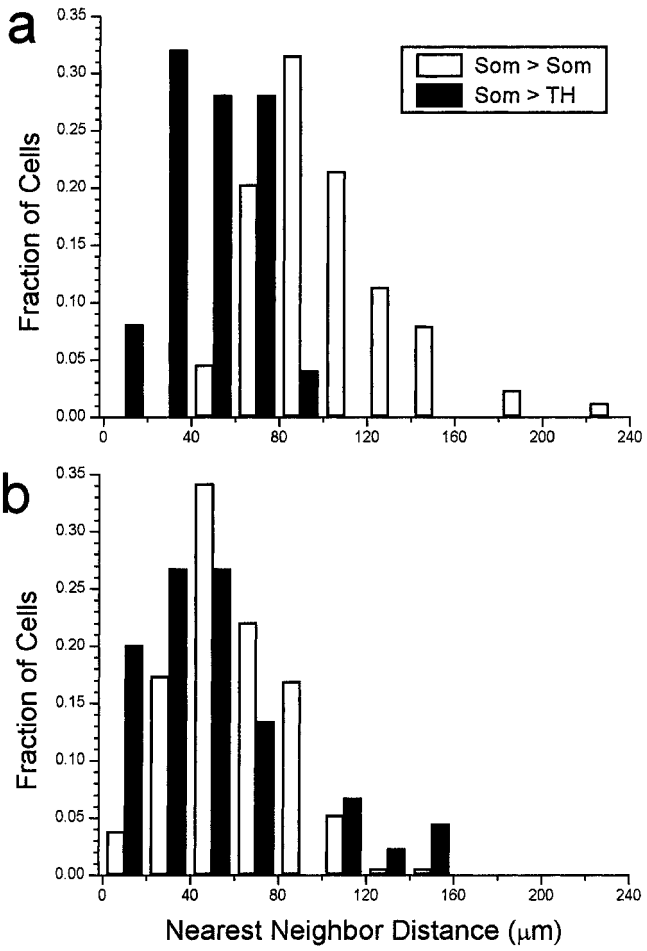

Fig. 8. Independence of distinct inner retinal cell mosaics in native and regenerated retina of zebrafish. **a:** NND distributions of anti-somatostatin-positive neurons to each other (open bars, from Fig. 4) and to anti-tyrosine hydroxylase-positive cells (solid bars) for native retina. Conformity ratio analysis revealed that most like-cell NND distributions in native retina are non-random, whereas unlike-cell NND distributions, such as that illustrated here, are typically not significantly different from those expected for random groups (cf. Tables 1 and 2). **b:** NND distributions as in a, for regenerated retina. In regenerated retina both like- and unlike-cell NND distributions tend toward randomness, with the latter typically being insignificantly different from random (Table 2).

was lower than the values for the corresponding like-cells (cf. Tables 1 and 2), and in most cases the conformity ratio analysis indicated that the unlike cell pairs were distributed randomly with respect to each other. These results indicate that the mosaic patterns of unlike inner retinal cell groups are largely independent of one another, and suggest that interactions between these unlike cell groups may not contribute significantly to the formation of their respective mosaic patterns.

Mosaic patterns in regenerated retina

Differentiation between native and regenerated retina could be readily achieved in retinal whole mounts by visual inspection of the underlying cone photoreceptor mosaic. The cone mosaic structure of native zebrafish retina is characterized by a very regular two-dimensional pattern of single and double cones (Fig. 2b; Larison and BreMiller, 1990; Raymond et al., 1995), whereas the cone mosaic of regenerated retina is significantly disrupted (Fig. 2c). This disruption is similar to that described previously for regenerated retina in laser-damaged goldfish retina (Braisted et al., 1995) and surgically-damaged sunfish retina (Cameron and Easter, 1995).

Two types of mosaic pattern anomalies were observed in regenerated retina. In the first, although most labeled cells within a given regenerated mosaic were coplanar, radial sections revealed occasional differences in radial cellular placement (Fig. 9a,b). These differences, which were not restricted to a single cell group, typically had the form of cell placement at an anomalous location within the appropriate nuclear layer. Second, inspection of retinal whole mounts revealed cases in which two like-cells were closely, and in some cases apparently directly, juxtaposed (Fig. 9c,d). These results indicate that during retinal regeneration, the assembly of inner retinal cell mosaics manifests a certain degree of spatial disruption relative to normal growth and development. Furthermore, the results also indicate that direct soma contacts between like-cells may not significantly regulate mosaic pattern formation during retinal regeneration.

All of the inner retinal cell groups observed in native retina were also observed in regenerated retina. Cell densities in regenerated retina were greater than in native retina (Table 1), as previously reported for cones (Cameron and Easter, 1995) and tyrosine hydroxylase-positive cells (Hitchcock and VanDeRyt, 1994) in other species. Like their counterparts in native retina, the NND distributions for most cell groups in regenerated retina were well estimated by Gaussian functions (solid bars and dashed lines, Figs. 4 and 5; Table 1). Similarly, these NND distributions were not well estimated by the Rayleigh function. The conformity ratio analysis indicated that all of the cell mosaics in regenerated retina, with the exception of anti-neuropeptide Y- and anti-substance P-positive cells, were significantly different from uniformly distributed random distributions ($P < 0.05$; filled bars, Fig. 6b). With the exception of anti-GABA-positive cells, these ratios were always less than the corresponding values for native retina. Because care was taken to restrict analysis of GABA-positive cells only to those cells along the border of the inner nuclear and inner plexiform layers, the irregular radial distribution of cells in regenerated retina (Fig. 9a,b) could have resulted in an under-sampling of GABA-positive cells. For the regenerated GABA-positive cells, this methodological restriction could result in an over estimate of both the NND and conformity ratio values, and an underestimate of the cellular density. However, of these measures, only the conformity ratio of GABA-positive cells deviated from the native/regenerated trend manifest by the other cell groups (Table 1).

The computer-generated random distributions, matched to the density of a given regenerated cell group, always had lower conformity ratios and were always insignificantly different from theoretical uniform distributions (Table 1; Cook, 1996). These results indicate that the cell mosaic patterns in regenerated zebrafish retina are largely non-random, but that compared to their counterparts in native retina, the regenerated mosaics typically tend toward greater densities (Table 1), lower mean NND values (Fig. 6a), and less "tight" two-dimensional organization (Fig. 6b). These differences between native and regenerated mosaics support the hypothesis that the assembly

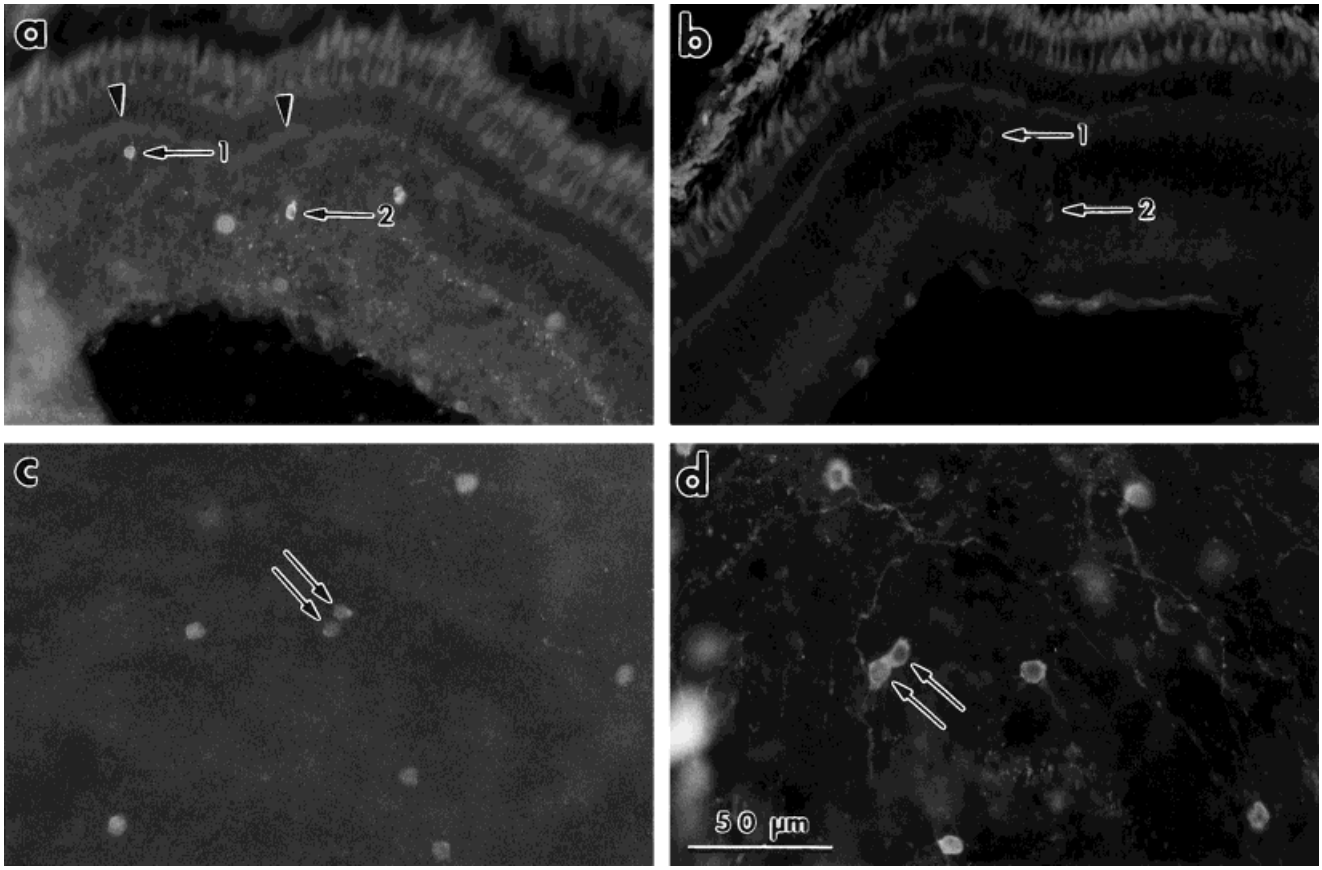

Fig. 9. Anomalous cell distributions in regenerated zebrafish retina. **a:** Anti-serotonin-positive cells located at disparate depths within the inner nuclear layer. The labeled cell marked "1" is much closer to the distal edge of the inner nuclear layer (nearby arrowhead) than the labeled cell marked "2," the latter having a location similar to that associated with anti-serotonin-positive cells in native retina (Fig. 2a). **b:** Anti-tyrosine hydroxylase-positive cells located at disparate depths within the inner nuclear layer of regenerated retina ("1" and "2"). **c:** Anti-serotonin-positive cells within regenerated retina, viewed in a whole mount. The indicated, coplanar, labeled cells (arrows) are within 3 μm of each other, much closer than ever observed in native retina (Fig. 5). **d:** Anti-tyrosine hydroxylase-positive cells in regenerated retina that, at this level of resolution, are directly juxtaposed (arrows). Such directly juxtaposed cells were not observed in native retina (Fig. 4).

of cell mosaics during retinal regeneration represents a spatially disrupted recapitulation of the neurogenerative mechanisms that operate during normal retinal growth and development.

Like the native retina mosaics, the DRP analysis revealed that regenerated mosaics (save for propidium iodide-positive cells) are characterized by anti-clustering (Fig. 7, Table 1), and provide additional evidence for non-random spatial patterns in regenerated mosaics. With the sole exception of anti-serotonin-positive cells, the calculated effective radius values for each cell group in regenerated retina were always smaller than the corresponding values for native retina (Table 1), consistent with the higher cellular densities in regenerated retina.

NND analysis was utilized to assay for independence between the mosaics of unlike cell groups in regenerated retina (Fig. 8b). The resultant conformity ratios for unlike-cells were always lower than the values for the corresponding like-cells in regenerated retina (Fig. 6b; cf. Tables 1 and 2), and they were also lower than the ratio for the corresponding unlike-cell pair in native retina (Table 2), consistent with the interpretation that cell mosaics in regenerated retina are spatially disrupted. Additionally, because the conformity ratio analysis revealed that the NND distributions between unlike-cells in regenerated retina were always random (with the exception of anti-PKC → anti-tyrosine hydroxylase-positive cells, which was nearly so; Table 2), a spatial independence between disparate cellular mosaics in regenerated retina was inferred. Perhaps most significantly, the results suggest that during both retinal growth and regeneration, direct soma contacts between unlike neurons may not significantly regulate the formation of cellular mosaic patterns in the zebrafish inner retina.

DISCUSSION

Formation of non-random cellular patterns

The stereotypical, stratified cellular organization of the vertebrate retina defines it as an attractive system for investigating the assembly of neural structures during development. Since the pioneering work of Hannover (1840), the retinas of adult teleost fish have also been known to possess cellular patterns that are highly ordered within the tangential plane of the retina, including the

inner retina (e.g., Van Haesendonck and Missotten, 1991; Van Haesendonck et al., 1993), but particularly at the level of cone photoreceptors in the outer retina. Investigators such as Müller (1952) and Lyall (1957) recognized the interpretive power of the non-random cone photoreceptor mosaics of teleosts toward understanding the developmental assembly of the neural retina, and ongoing investigations of pattern formation in the outer retina of developing fish continue to enhance this understanding (e.g., Raymond et al., 1995; Schmitt and Dowling, 1996; Stenkamp et al. 1996; Stenkamp et al., 1997).

The current report builds upon these earlier studies by providing quantitative analyses of the spatial organization of eight distinct cell groups in the inner retina of adult zebrafish. Because the labeling techniques utilized in this study do not necessarily label cells of a common "type" (e.g., all subtypes of RGCs are likely to be labeled by the propidium iodide technique), our interpretations of the data are restricted solely to cells of a given group (see Materials and Methods). However, a principal feature common to most cell groups analyzed, which likely includes examples of amacrine, bipolar, and retinal ganglion cells, is that the two-dimensional pattern of each distinct cell group is non-random. This general feature of retinal organization argues that the assembly of not only the radial, but also the tangential, plane of the neural retina is spatially organized. The results can not rule out the operation of spatially random mechanisms during retinal neurogenesis, but if they are operational, their intrinsically random spatial attributes are overcome by the spatial organizing mechanisms.

What is the nature of these non-random, spatial organizing mechanisms? The presence of like-cell-free zones of exclusion around the individual somata of most cell groups implies the operation of some laterally-acting, self-inhibitory mechanism(s) during development, growth, and regeneration. This interpretation may be consistent with the results from studies of the zebrafish mutant *cyclops*, which have suggested that local interactions between cells might regulate retinal cell patterning (Fulwiler et al., 1997). Local, laterally-acting mechanisms are likely to represent a general developmental theme; for example, they are reminiscent of the lateral mechanisms that regulate neuronal differentiation and pattern formation during the development of the *Drosophila* eye (review: Sawamoto and Okano, 1996). Because the effective radius values (i.e., the "sphere of influence" of the inhibitory mechanisms) inferred from the DRP analyses were typically significantly larger than each cell's somatic diameter, the self-inhibitory, anti-clustering cues may involve diffusible signaling mechanisms.

Because the mosaic patterns of different retinal cell groups were largely independent of each other (Fig. 8, Table 2), it seems unlikely that a single, signal/receptor mechanism common to all cell groups could account for the self-inhibitory mechanism. Of potential significance to this issue are the occasional "errors" in the assembly of cell mosaics during retinal regeneration, in which two like-cells are directly juxtaposed, or very nearly so (Fig. 9c, d). Such errors in mosaic pattern formation suggest that the inferred self-inhibitory mechanism(s) are either locally absent or are somehow masked. However, the errors also suggest that soma-contact-mediated inhibitory mechanisms, even between like-cells, may not significantly regulate the establishment of cell mosaic patterns in regenerated retina; if they had, no two like-cells should ever have been so closely juxtaposed as in Figure 9c,d.

The results also suggest potential mismatches between mosaic patterns of retinal neurons that are synaptically associated. The location and size of the bulbous axon terminals of the anti-PKC-positive cells in this study suggest that many of these cells are likely to be rod-associated, ON-type bipolar cells (Suzuki and Kaneko, 1990). The spatial organization of these putative rod-associated cells (Fig. 1a) is, apparently, significantly different from that of the rod photoreceptors, the latter having an organized mosaic pattern early in development but a rather disorganized mosaic pattern in the adult (Stenkamp et al., 1996). We interpret this potential spatial mismatch in the adult retina as resulting from the life-long addition of rod photoreceptors to the central adult retina. We hypothesize that early in retinal development the mosaics of rods and their associated bipolar cells may be in spatial register, perhaps being organized in tandem due to common lineage or the action of some other spatial organization mechanism(s) common to the two cell groups. However, as rods (but not bipolar cells) are added to the central retina via rod precursor cells during the life of the animal (Johns and Fernald, 1980; Raymond and Rivlin, 1987), the rod mosaic pattern becomes progressively disorganized. Because such newly added rods are likely to contribute to vision (Powers et al., 1988), it is evident that visual function is not necessarily dependent upon a static, precise spatial registration between the somata of synaptically-associated retinal neurons in two-dimensional space. It thus follows that spatial dissociation between the mosaic patterns of synaptically-associated neurons in regenerated retina does not necessarily preclude the regenerated structure from restoring visual function.

Regeneration vs. development

Two characteristic, although somewhat mysterious, features of the adult teleost retina are its ability to grow throughout life, and its ability to regenerate following injury. One of the manifestations of life-long retinal growth (the production of new neurons) has been argued to be inextricably linked to the fish retina's ability to regenerate neurons (Raymond and Hitchcock, 1997; Huang and Sato, 1998). Conceptually, the adaptive significance for retinal regeneration seems obvious: the restoration of visual function that is lost due to retinal trauma or disease. But the underlying cellular issue of whether, and to what extent, retinal regeneration is a recapitulation of retinal development remains somewhat less clear.

The results from the current study argue that following surgical extraction of a small piece of an adult teleost retina, the damaged retina reinitiates a complex array of cellular and molecular events that operate during development. How this regenerative process is triggered at the molecular level is unknown, but the cellular outcomes of retinal development and regeneration are remarkably, and perhaps non-coincidentally, similar. For example, all neuronal cell groups identified in native retina are also observed in regenerated retina, and their cellular mosaic patterns are almost always non-random. It is clear that significant errors in cellular pattern formation are made during retinal regeneration, mistakes that could directly influence the ability of the regenerated structure to restore visual function: cellular mosaics have higher densities than normal and tend toward randomness (Figs. 4–6, and

Table 1), cellular mosaics possess misplaced cells (Fig. 9), and atypical cone morphologies are prevalent (Cameron and Easter, 1995). However, given the empirical evidence from earlier studies that have shown that the radial stratification pattern, synaptic architecture, and visual pigment content of regenerated retina is largely similar to that of native retina, it seems likely that retinal regeneration could be driven by the same neurogenetic mechanisms that operate during normal retinal development, albeit with a significant degree of spatial disruption.

ACKNOWLEDGMENTS

We thank Dr. Carter Cornwall and Dr. Deborah Stenkamp for discussions and comments regarding the manuscript. This work was supported by National Institutes of Health grant EY11160 (D.A.C.).

LITERATURE CITED

Boucher S-EM, Hitchcock PF. 1998. Insulin-related growth factors stimulate proliferation of retinal progenitors in the goldfish. J Comp Neurol 394:386–394.

Braisted JE, Essman TF, Raymond PA. 1995. Selective regeneration of photoreceptors in goldfish retina. Dev Brain Res 76:221–232.

Cameron DA, Easter SS Jr. 1993. The cone photoreceptor mosaic of the green sunfish (*Lepomis cyanellus*). Visual Neurosci 10:375–384.

Cameron DA, Easter SS Jr. 1995. Cone photoreceptor regeneration in adult fish retina: phenotypic determination and mosaic pattern formation. J Neurosci 15:2255–2271.

Cameron DA, Cornwall MC, MacNichol EF Jr. 1997. Visual pigment assignments in regenerated retina. J Neurosci 17:917–923.

Cameron DA, Vafai H, White JA. 1999. Analysis of dendritic arbors of native and regenerated ganglion cells in the goldfish retina. Visual Neurosci 16:253–261.

Clark PJ, Evans FC. 1954. Distance to nearest neighbor as a measure of spatial relationships in populations. Ecology 35:445–453.

Cook JE. 1996. Spatial properties of retinal mosaics: an empirical evaluation of some existing measures. Visual Neurosci 13:15–30.

Dowling JE. 1987. The Retina: an approachable part of the brain. Belknap: Cambridge, MA. 1987.

Ehinger B, Dowling JE. Retinal neurocircuitry and transmission. In: Björklund A, Hökfelt T, Swanson LW, editors. Handbook of chemical neuroanatomy. Elsevier: Amsterdam. p 389–446.

Fulwiler C, Schmitt EA, Kim JM, Dowling JE. 1997. Retinal patterning in the zebrafish mutant *cyclops*. J Comp Neurol 381:449–460.

Graw J. 1996. Genetic aspects of embryonic eye development in vertebrates. Dev Genet 18:181–197.

Hannover A. 1840. Ueber die Netzhaut und ihre Gehirnsubstanz bei Wirbelthieren, mit Ausnahme des menschen. Archiv Anat Physiol Wissenschaftliche Medicin 320–345.

Hitchcock PF. 1997. Tracer coupling among regenerated amacrine cells in the retina of the goldfish. Visual Neurosci 14:463–472.

Hitchcock PF, Cirenza P. 1994. Synaptic organization of regenerated retina in the goldfish. J Comp Neurol 343:609–614.

Hitchcock PF, VanDeRyt JT. 1994. Regeneration of the dopamine-cell mosaic in the retina of the goldfish. Visual Neurosci 10:209–218.

Hitchcock PF, Macdonald RE, VanDeRyt JT, Wilson SW. 1996. Antibodies against Pax6 immunostain amacrine and ganglion cells and neuronal progenitors, but not rod precursors, in the normal and regenerating retina of the goldfish. J Neurobiol 29:399–413.

Hitchcock PF, Lindsey Myrh KJ, Easter SS Jr., Mangione-Smith R, Jones DD. 1992. Local regeneration in the retina of the goldfish. J Neurobiol 23:187–203.

Huang S, Sato S. 1998. Progenitor cells in the adult zebrafish nervous system express a Brn-1- related POU gene, tai-ji. Mechanisms Dev 71:23–35.

Johns PR, Fernald RD. 1981. Genesis of rods in teleost fish retina. Nature 293:141–142.

Kock J-H, Reuter T. 1978. Retinal ganglion cells in the crucian carp (*Carassius carassius*). J Comp Neurol 179:535–548.

Larison KD, BreMiller R. 1990. Early onset of phenotype and cell patterning in the embryonic zebrafish retina. Development 109:567–576.

Lyall AH. 1957. Cone arrangements in teleost retinae. Quart J Microscop Sci 98:189–201.

Marshak DW, Yamada T, Stell WK. 1984. Synaptic contacts of somatostatin-immunoreactive amacrine cells in goldfish retina. J Comp Neurol 225:44–52.

Müller H. 1952. Bau und Wachstum der Netzhaut des Guppy (*Lebistes reticulatus*). Zoologische Jahrbuecher (Zoolog Physiolog) 63:275–324.

Powers MK, Bassi CJ, Rone LA, Raymond PA. 1988. Visual detection by the rod system in goldfish of different sizes. Vision Res 28:211–221.

Raymond PA, Hitchcock PF. 1997. Retinal regeneration: common principles but a diversity of mechanisms. Adv Neurol 72:171–184.

Raymond PA, Rivlin PK. 1987. Germinal cells in the goldfish retina that produce rod photoreceptors. Dev Biol 122:120–138.

Raymond PA, Barthel LK, Curran GA. 1995. Developmental patterning of rod and cone photoreceptors in embryonic zebrafish. J Comp Neurol 359:537–550.

Raymond PA, Reifler MJ, Rivlin PK. 1988. Regeneration of goldfish retina: rod precursors are a likely source of regenerating cells. J Neurobiol 19:431–463.

Rodieck RW. 1991. The density recovery profile: a method for the analysis of points in the plane applicable to retinal studies. Visual Neurosci 6:95–111.

Rodieck RW. 1998. The First Steps in Seeing. Sinauer: Sunderland, MA. Sawamoto K, Okano H. 1996. Cell-cell interactions during neural development: multiple types of lateral inhibitions involved in *Drosophila* eye development. Neurosci Res 26:205–214.

Schmitt EA, Dowling JE. 1996. Comparison of topographical patterns of ganglion and photoreceptor cell differentiation in the retina of the zebrafish, *Danio rerio*. J Comp Neurol 371:222–234.

Stenkamp DL, Barthel LK, Raymond PA. 1997. Spatiotemporal coordination of rod and cone photoreceptor differentiation in goldfish retina. J Comp Neurol 382: 272–284.

Stenkamp DL, Hisatomi O, Barthel LK, Tokunaga F, Raymond PA. 1996. Temporal expression of rod and cone opsins in embryonic goldfish retina predicts the spatial organization of the cone mosaic. Investigative Ophthalmol Visual Sci 37:363–376.

Suzuki S, Kaneko A. 1990. Identification of bipolar cell types by protein kinase C-like immunoreactivity in the goldfish retina. Visual Neurosci 5:223–230.

Van Haesendonck E, Missotten L. 1991. Patterns of glutamate-like immunoreactive bipolar cell axons in the retina of the marine teleost, the dragonet. Vision Res 31:451–462.

Van Haesendonck E, Marc RE, Missotten L. 1993. New aspects of dopaminergic interplexiform cell organization in the goldfish retina. J Comp Neurol 333:503–518.

Wässle H, Riemann HJ. 1978. The mosaic of nerve cells in the mammalian retina. Proc R Soc London B 200:441–461.

Yazulla S. 1986. GABAergic mechanisms in the retina. Prog Retinal Res 5:1–32.

Yazulla S, Zucker CL. 1988. Synaptic organization of dopaminergic interplexiform cells in the goldfish retina. Visual Neurosci 1:13–29.

Yazulla S, Studholme KM, Zucker CL. 1985. Synaptic organization of substance P-like immunoreactive amacrine cells in goldfish retina. J Comp Neurol 231: 232–238.